A Low-Power Dual-Frequency RF Front-End Architecture for GNSS Receivers

Frederic Chastellain, Cyril Botteron, Pierre-Andre Farine

***Abstract*— With the availability in the years to come of several new Global Navigation Satellite Systems transmitting signals located in different frequency bands, the question of the feasibility of multi-frequency receivers aimed at the mass market is of major interest. Most solutions proposed today either use single-frequency receivers in parallel or directly sample the signals at the antenna, two solutions which are not applicable to the mass market. In this paper, a dual-frequency RF front-end architecture with a similar power-consumption and complexity as current state-of-the-art single-frequency front-ends is proposed. It is based on a super-heterodyne architecture and exploits the fact that the L1C/A and L2C signals only occupy 2 MHz of the 20 MHz L1 and L2 bands to allow the simultaneous acquisition and tracking of both the L1C/A and L2C signals.**

***Index Terms*—GNSS, front-end, dual-frequency, low-power, architecture**

I. Introduction

Today, the majority of Global Positioning System (GPS) receivers use the L1C/A signal, the only civil signal currently transmitted by a full constellation of satellites, to compute their position. The United States' GPS is actually only one of several Global Navigation Satellite Systems (GNSS) under development, such as the European Galileo or the Japanese Quasi-Zenith Satellite System (QZSS). In the years to come, the constellations of these new GNSS will be fully deployed, providing new modernized signals. The GPS is actually also being modernized and will provide two new civil signals, the first in the L2 band (1227.6 MHz) and the second in the L5 band (1176.45 MHz), as well as an improved version of the L1C/A signal in the L1 band (1575.42 MHz). The first fully available new civil signal will be the GPS civil signal in the L2 band called the L2C signal.

The availability of several civil signals in different bands will allows improving the performances of current receivers by offering, for example, a better accuracy, availability and reliability in difficult indoor or urban canyons environments. However, receiving signals located in different bands will add complexity in the receiver, particularly in the radio-frequency (RF) front-end. This is a major issue since, for the mass market, improved performances do usually not justify a higher power consumption and cost.

Contact's address: Cyril Botteron, Electronics and Signal Processing Laboratory (ESPLAB), IMT-STI-EPFL, Neuchâtel, Switzerland (phone: +41 32 718 3424; e-mail: cyril.botteron@epfl.ch);

In this paper, a dual-frequency RF front-end architecture for the L1C/A, L2C and Galileo $E1_{b,c}$ signals that can be integrated using standard CMOS technology and which has a power consumption comparable with that of state-of-the-art single-frequency GPS RF front-ends is presented.

A. The GPS L1C/A and L2C signals

The L1C/A and L2C signals are both generated using binary phase-shift keying (BPSK) based direct-sequence spread spectrum (DS-SS) modulation. The E1b,c signal is uses Binary Offset Carrier (BOC) modulation. The main characteristics of the three signals are recalled in Table I.

Table I: main characteristics of the L2C, L1C/A, $E1_b$ and $E1_c$ signals.

Parameter	*Unit*	*L2CM*	*L2CL*	*L1C/A*	*E1b*	*E1c*
Code length	chips	10230	767250	1023	8184	8184·25
Code rate	kHz	511.5	511.5	1023	1023	1023
Symbol rate	ms	20	None	20	4	None
Data rate	Hz	25	No data	50	125	No data
BW	MHz	2	2	2	4	4

II. Existing solutions

A. Review Stage

The solution most commonly met to implement a multi-frequency GNSS front-end consists to replicate a single-frequency front-end for each signal to be acquired. This certainly works for high-end receivers but is not applicable for those aimed at the mass market. Similarly, solutions based on direct-sampling or bandpass-sampling of the RF signals don't suit the mass market due to the high sampling rates involved [1].

When only two signals need to be processed by the front-end, a possible approach consists to use an (super-)heterodyne architecture with the signals as image one of each other or, equivalently, with the local oscillator (LO) frequency f_{lo} in-between the two signals. In this case, it is possible to downconvert both signals to an intermediate frequency (IF) with a single common RF mixer and LO. Clearly, since the IF is not equal to zero, at least one additional downconversion stage is required.

The first decision to make is whether the RF mixer is real or complex. In the complex case, the signals are multiplied by $\exp(-j2\omega f_{lo1}t)$, where $f_{lo1} = (f_{l1}+f_{l2})/2 = 1401.51$ MHz. As a result, L1C/A is downconverted to 173.91 MHz and L2C to -173.91 MHz, a first IF which is still too high to make the A-

to-D conversion of the signals at this point a suitable option. If the RF mixer is then followed by a set of real IF mixers and their outputs summed, the resulting architecture is similar to Weaver's detector [2]. Since the two signals are image of each other, either L1C/A or L2C is selected by summing or subtracting the outputs of the IF mixers. Unfortunately, since the output of the Weaver architecture is real, it can't be used to demodulate complex baseband signals or real signals containing a Doppler component. If the second frequency translation is complex, two additional complex IF mixers are required. The resulting architecture, similar to the wideband-IF double-conversion architecture [3], requires a complex RF mixer, two complex IF mixers and four ADCs, making it a poor candidate to implement a low-power, highly-integrated dual-frequency receiver. Using a real RF mixer followed by a complex IF mixer reduces the complexity to that of a single-frequency super-heterodyne front-end. However, if f_{lo1} is kept equal to 1401.51 MHz, the signals are image one of each other and the images can't be filtered (Figure 1(a)). As a consequence, even if no strong interferer is present, the unfiltered thermal noise at the image frequencies still results in a SNR degradation of up to 3 dB. This solution is therefore not applicable for GNSS receivers due to their tight noise budget. It can be used though if the two signals do not have to be processed simultaneously, as proposed in [4], where the front-end's input is preceded by a switch which allows selecting either an L1 or an L2 antenna/filter combination. The published power consumption in [4] is 19 mW from a 1.8 V supply, which is comparable to the power consumption of state-of-the-art single-frequency front-ends implemented in the same technology such as [5] or [6]. This is very promising from a power consumption point of view but still doesn't allow the acquisition of both signals simultaneously!

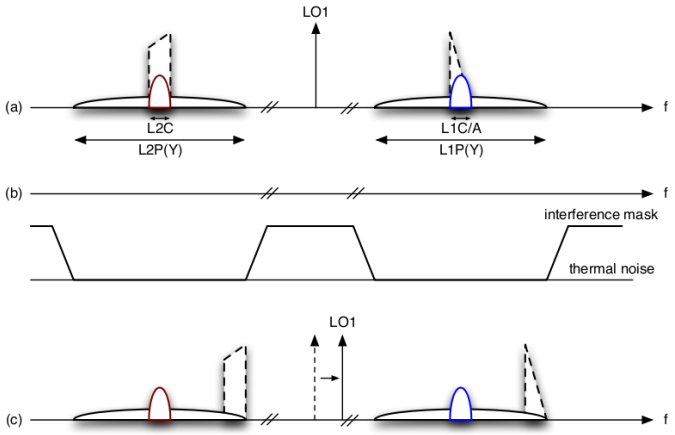

Figure 1: (a) signals and images when flo1=1401.51 MHz, (b) interference mask and thermal noise level, (c) signals and images when the LO is slightly shifted.

III. PROPOSED SOLUTION

To overcome the limitations presented in the previous section, we use the principle presented in [7]: in the L1 and L2 bands, the GPS civil signals only occupy 2 MHz of the 20 MHz allocated to the military signals in the same bands (Figure 1(a)). In these 20 MHz, the interference mask level is comparable to the thermal noise level (Figure 1(b)). As a consequence, if the LO is shifted from 1401.51 MHz while keeping the images in the military bands (Figure 1(c)), the images can be considered as limited to thermal noise, drastically reducing the required image rejection ratio (IRR). f_{lo1} should therefore satisfy the following inequality

$$1397.01 < f_{lo1} < 1406.1, \quad (1)$$

which ensures that the images lie in either the L1 or the L2 band. At this point, the NF is still degraded by 3dB by the first downconversion if the images are not filtered. This is not the case though if the LO shift is sufficient to push the images outside of the RF filters' bandwidth. As a consequence, the LO shift should not only satisfy (1) but also be maximized. Also, in order to minimize the architecture's complexity, the second LO should be derived from the first LO. Finally, using digital quadrature sampling [8] with

$$f_s = kf_{if\,2,li} = kmf_{if\,2,lj}, \quad (2)$$

where k and m are integers, $f_{if2,li}$ is the second IF of the l_i signal and $f_{if2,lj}$ is the second IF of the l_j signal, allows simplifying the demodulation.

The proposed frequency plan is represented in Table II. We have chosen f_{lo1} equal to 1407.648 MHz and $f_{lo2} = f_{lo1}/8 =$ 175.956 MHz, which results in $f_{if2,l1}$ and $f_{if2,l2}$ equal to 8.184 MHz and 4.092 MHz, respectively. The frequency plan's reference frequency f_{ref} is 16.368 MHz and since f_{lo1} is an integer multiple of f_{ref}, the phase noise contribution of the PLL is minimized. The proposed frequency plan also satisfies (1.2) with k = 2 and m = 2. f_{lo1} is slightly above the limit set by (1.1). Nevertheless, since the interference mask is not a brickwall function, it does not lead to any SNR degradation. Also, since 16.368·75 = 1227.6 MHz, the front-end should be carefully designed in order to avoid self-interference.

Table II: proposed frequency plan for an L1C/A + L2C low-power front-end.

Signal	*RF*	*LO1*	*IF1*	*LO2*	*IF2*
L1C/A	1575.42	1407.648	167.772	175.956	8.184
L2C	1227.60	1407.648	180.048	175.956	4.092

The front-end's architecture is represented in Figure 2. The signals are first amplified by a wideband or dual-band LNA and filtered by a dual-band bandpass filter. They are then translated to their respective first IF by a single real mixer. Since the second mixer is complex, no highly selective IF1 filter is required to attenuate the images at this point. A 3rd order Butterworth filter with a 90 MHz bandwidth and implemented off-chip with SMD components is used instead, mostly to attenuate the signals' energy upconverted by the RF mixer. The signals are translated to their second IF using a complex IF mixer and lowpass filtered using a 5th order

Chebyshev active lowpass filter (LPF) with a cut-off frequency of 10.184 MHz.

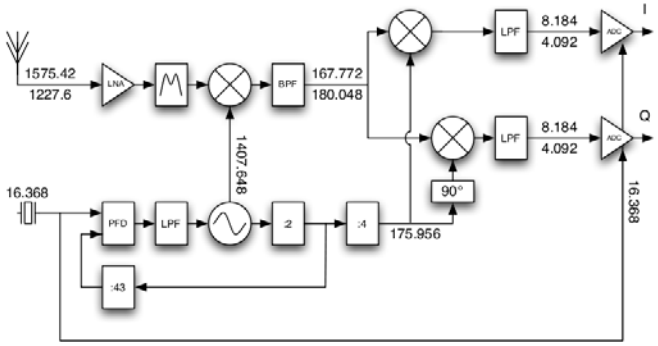

Figure 2: simplified schematic of the proposed dual-frequency L1C/A + L2C architecture.

The signals are then A-to-D converted. L1C/A is multiplied by $\exp(-j2\omega f_{if2,l1}t)$, which translates, in the digital domain, into

$$e^{-jn\pi} = \cos(n\pi) - \sin(n\pi) = (-1)^n. \tag{3}$$

It can therefore be implemented as a simple multiplication by $(-1)^n$ in the I path. L2C is multiplied by $\exp(j2\omega f_{if2,l2}t)$, which translates, in the digital domain, into

$$e^{-jn\frac{\pi}{2}} = \cos\left(n\frac{\pi}{2}\right) + j\sin\left(n\frac{\pi}{2}\right). \tag{4}$$

and can be implemented as a simple multiplication by [1; 0;-1; 0] in the I path and by [0; 1; 0;-1] in the Q path.
Since the BOC(1,1) component of the Galileo $E1_{b,c}$ signal uses the same carrier frequency as the L1C/A and has a 4 MHz bandwidth, it is also possible to process it using the proposed front-end.

A. *Specifications*

The specifications used for the validation of the architecture are reported in Table IV. They have been derived using the information in the GPS Standard Positioning Service (SPS) Performance Specifications (PS) document[1]. The minimum received signal power S_{min} defined in the SPS-PS is -130 dBm and the thermal noise power at the antenna N_{ant} is given by

$$\begin{aligned} N_{ant} &= 10\log(kT) + 10\log(B_{FE}) \\ &= -174dBm/Hz + 70dB = -104dBm, \end{aligned} \tag{5}$$

where the front-end's bandwidth B_{FE} is defined by the 10.184 MHz active LPF. Since the Signal-to-Noise Ratio at the antenna SNR_{ant}, in dB, is negative, the front-end's nominal gain is set to amplify N_{ant} up to the ADC's Full Scale Range (FSR). The noise figure (NF) is determined by S_{min}, the integration time t_{int}, as well as the minimum energy per bit to noise ratio $(E_b/N_0)_{min}$ required to achieve a target probability of detection P_d and false alarm P_{fa} for the modulation used. For S_{min} = -130 dBm, $(E_b/N_0)_{min}$ = 9.6 dB and t_{int} = 1 ms, we find

$$\begin{aligned} NF &= S_{\min} - 10\log(kT) - (E_b/N_0)_{\min} - 10\log(1/t_{\text{int}}) \\ &= 4.4dB. \end{aligned} \tag{6}$$

Other specifications such as the 3rd order Intercept Point (IP3) and phase noise (PN) are not found directly in the SPS-PS document. We have then set the IP3 and PN specifications so that the increase of the noise power due to the combined in-band interferers, out-of-band interferers and PN is not larger than 3dB[2]. For this design, the contributions of in-band interferers, out-of-band interferers and phase noise have been set to 40%, 40% and 20%, respectively. The input-referred 3rd order intercept point (IIP3) is computed using

$$IIP3 = \frac{3P_{\text{int}} - P_{IM3}}{2}, \tag{7}$$

where P_{int} is the power of the interferer and P_{IM3} is the power of the 3rd order intermodulation product (IM3).
The thermal noise power being

$$\begin{aligned} N_{th} &= 10\log(kTB_{FE}) = -174dBm/Hz + 10\log(10e6) \\ &= -104dBm, \end{aligned} \tag{8}$$

the maximum noise power, including the interferers and phase noise contributions, is given by

$$N_{th+i} = N_{th} + 3dB = -101dBm. \tag{9}$$

The resulting maximum allowed noise power added by the different contributors is reported in Table III.

Table III: maximum allowed noise power added by the different contributors.

Source	*Notation*	*Noise power*	*Unit*
Thermal noise	N_{th}	-104	dBm
In-band interferer	$P_{IM3,in}$	-108	dBm
Out-of-band interferer	$P_{IM3,out}$	-108	dBm
Phase-noise	N_{PN}	-111[3]	dBm

1) *In-band IP3 specification*

To compute the in-band IP3, we have used the in-band interference level defined in the TUSREQ document as -111.3 dBm/MHz. For a 10.184 MHz bandwidth, we get

$$\begin{aligned} P_{\text{int},in-band} &= -111.3dBm/MHz + 10\log(10e6/1e6) \\ &= -101.3dBm \end{aligned} \tag{10}$$

and the resulting in-band IIP3 is given by

[1] When not available, we have also used the Galileo Test User Requirement (TUSREQ) document.

[2] This approach is commonly used for other wireless communication standards.

[3] or equivalently, $N_{0,PN}$ = -181 dBm/Hz.

$$IIP3_{in-band} = \frac{3P_{\text{int},in-band} - P_{IM\,3,in}}{2} = \frac{3(-101.3)-(-108)}{2} = -98dBm. \quad (11)$$

2) Out-of-band IP3 specification

We proceed similarly to compute $IP3_{\text{out-of-band}}$. Based on the Galileo TUSREQ document, the two strongest out-of-band interferers resulting in an IM3 falling in either the L1 or the L2 band are at 1620 MHz and 1664.58 MHz, and have a power of -60 dBm. We find

$$P3_{out-of-band} = \frac{3P_{\text{int},out-of-band} - P_{IM\,3,out}}{2} = \frac{3(-60)-(-108)}{2} = -36dBm. \quad (12)$$

3) Phase-noise specification

The phase noise, usually expressed in dBc/Hz, is defined by

$$PN\{\Delta f\} = 10\log\left(\frac{N_0\{\Delta f\}}{P_c}\right), \quad (13)$$

where P_c is the power of the oscillator's fundamental component at frequency f_c and $N_0\{\Delta f\}$ is the noise power spectral density (PSD) at a given offset frequency Δf from f_c. The phase noise requirement is computed by replacing in (13) the oscillator by the strongest interferer in the vicinity of the signal. The noise degradation due to the phase noise of the LO occurs after the signals and interferers are downconverted to their first IF. As a consequence, the noise and interferer power of interest are those at the input of the mixer. We have seen that the added noise PSD due to the phase noise is $N_{0,PN}$ = -181 dBm/Hz. The total gain in front-of the mixer being 27 dB, we find

$$N_{0,PN,mix-in} = N_{0,PN} + 27dB = -154dBm/Hz. \quad (14)$$

The strongest interferer located in the vicinity of the L1C/A signal is at 1550 MHz and has a power of -46.8 dBm, leading to

$$\Delta f = f_{L1} - BW_{L1}/2 - f_{\text{int}} = 1575,42 - 10 - 1550 = 15.42MHz. \quad (15)$$

For the worst case condition where all the active stages are wideband and the RF filters provide an attenuation of 27 dB at 1550 MHz, the interferer's power at the mixer's input is -46.8 dBm. Using (1.13), we find

$$PN\{15.42MHz\} = -154dBm/Hz - (-46.8dBm) = -107.2dBc/Hz. \quad (16)$$

Reciprocal mixing also occurs between the phase noise and the thermal noise, which results in an in-band phase-noise specification defined by

$$PN\{in-band\} = -154dBm/Hz - (-104dBm + 27dB) = -77dBc/Hz. \quad (17)$$

The front-end's target specifications are summarized in Table IV.

Table IV: target specifications of the proposed dual-frequency front-end.

Parameter		*Value*	*Unit*
G	>	95.9	dBV
NF	<	4.4	dB
$IIP3_{\text{in-band}}$	>	-98.0	dBm
$IIP3_{\text{out-of-band}}$	>	-36.0	dBm
PN{in-band}	<	-77.0	dBc/Hz
PN{15.42MHz}	<	-107.2	dBc/Hz
S11	<	-10	dB

B. Simulation

In order to validate the proposed architecture, the front-end has then been simulated at the system level using Genesys. An example of a schematic used in Genesys to validate the architecture is represented in Figure 3. In this case, we have created two separated RF paths in order to get simulation results for the L1C/A and L2C signals, simultaneously.

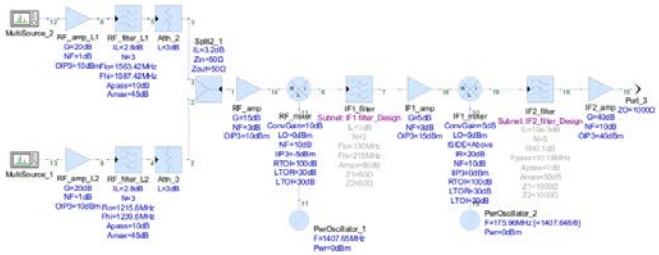

Figure 3: example of schematic implemented in Genesys to validate the proposed front-end architecture.

The front-end's CMOS circuits have been implemented using Genesys models with parameters extracted from prior art, such as [9] for the LNA or [5] for the second IF LPF. The RF filters have been modeled based on the response of commercially available SAW filters. For example, the L1 RF filter is JRC's NSVS658 and has been modeled as a 3rd order Chebyshev bandpass filter with a 2.8 dB insertion loss (IL), 10 dB bandwidth of 24 MHz and maximum attenuation of 45 dB. Its response is represented in Figure 4.

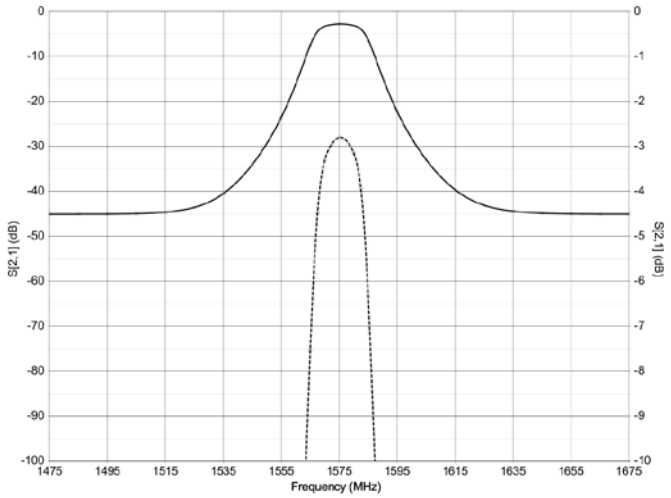

Figure 4: transfer function of the RF filter model for the L1 band.

For more specific circuits, the complete design has been implemented in Genesys. For example, the first IF filter is an external filter implemented with SMD capacitors and inductors. For this reason it has been simulated with measurement-based models of capacitors and inductors provided by their respective manufacturer. Also, as shown in Figure 5, Monte Carlo simulations have been performed to guarantee that the filter's specifications could be achieved despite the components' tolerances.

Figure 6 shows the simulated gain along the front-end, for the L1C/A and L2C signals. Figure 7 and Figure 8 show the simulated NF along the front-end, for the L1C/A and L2C signals, respectively. Such plots are very useful to identify quickly the potential sources of NF degradation in the front-end.

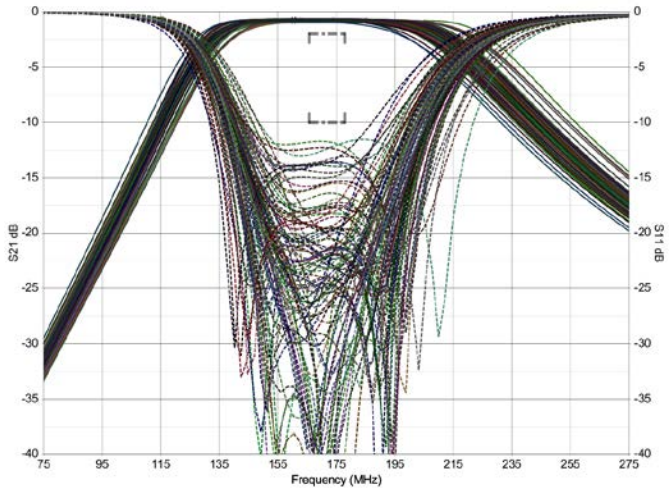

Figure 5: Monte Carlo analysis of the IF1 filter.

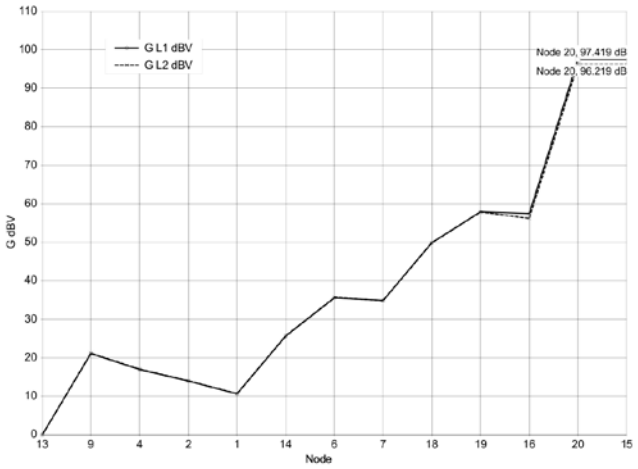

Figure 6: gain analysis for the L1C/A and L2C signals.

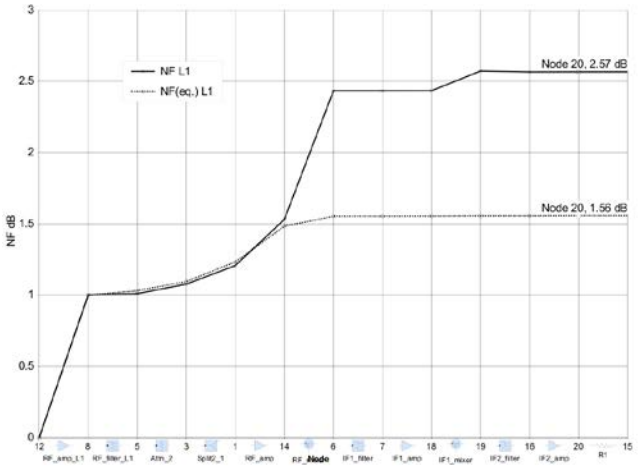

Figure 7: NF analysis for the L1C/A signal.

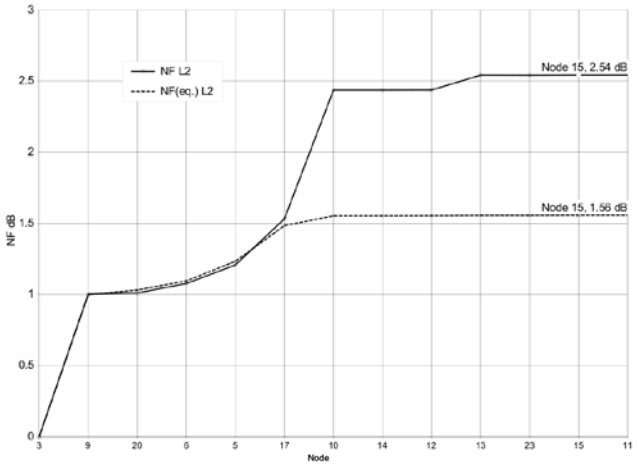

Figure 8: NF analysis for the L2C signal.

Figure 9 is another example of a simulation performed to validate the proposed architecture. It represents the power spectrum at the output of the front-end when the L1C/A and L2C as well as two -60 dBm interferers at 1620 MHz and 1664.58 MHz are injected in the front-end. This allows to

confirm that the generated IM3 falling at 8.184 MHz is indeed below the specified level and that no other strong intermodulation product or harmonic is present at 4.092 MHz and 8.184 MHz.

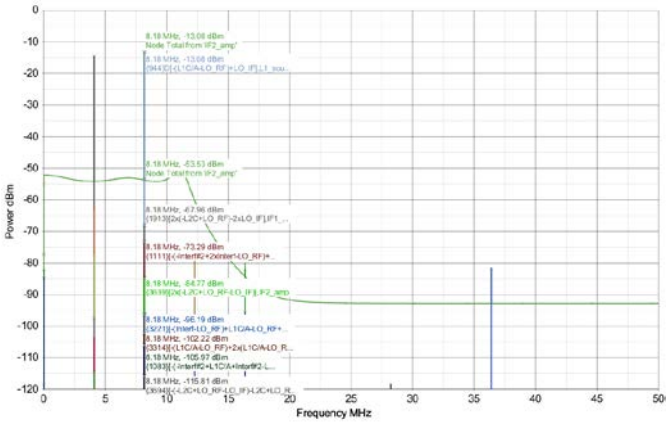

Figure 9: spectrum at the output of the front-end in the presence of two -60dBm interferers at 1620Mz and 1664.58Mz.

As we can see in Table V, the performances obtained by simulation satisfy each specification.

Table V: summary of the initial specifications and simulation results.

Parameter	Unit	Specification	Simulation	
			L1C/A	L2C
G	dBV	95.9	97.4	96.2
NF	dB	3.0	2.6	2.5
$IIP3_{in\text{-}band}$	dBm	-98.0	-53.6	-52.9
$IIP3_{out\text{-}of\text{-}band}$	dBm	-36.0	-10.7	-10.5

IV. CONCLUSION

We have presented a novel dual-frequency front-end architecture which allows acquiring and tracking the GPS L1C/A and L2C signals simultaneously and does not consume more power than state-of-the-art single-frequency front-ends. The architecture uses a single RF LO and RF mixer to downconvert both signals to baseband. This clearly reduces the power consumption and also minimizes the potential for harmful harmonics, intermodulation products and other spurious components. Since the first LO is not chosen exactly in between the two signals, both can be acquired simultaneously at no SNR loss. For most wireless communication standards, this would place stringent requirements on the front-end and more particularly on the RF filters. In the proposed architecture, since the images are chosen in the GPS military bands, they can be considered as limited to thermal noise which relaxes the IRR requirements to a great extent.

REFERENCES

[1] E. Rivera Parada, F. Chastellain, C. Botteron, Y. Tawk, P.-A. Farine, *Design of a GPS and Galileo Multi-Frequency Front-End*, IEEE 69th Vehicular Technology Conference, 2009.

[2] D. K.Weaver, *A Third Method of Generation and Detection of Single-Sideband Signals*, Proceedings of the IRE, pp.1703-1705, 1956.

[3] J. C. Rudell, J. J. Ou, T. B. Cho, G. Chien, F. Brianti, J. A. Weldon, P. R. Gray, *A 1.9-GHz Wide-Band IF Double Conversion CMOS Receiver for Cordless Telephone Applications*, IEEE Journal of Solid-State Circuits, vol.32, no.12, pp.2071-2088, 1997.

[4] J. Ko, K. Jongmoon, S. Cho, K. Lee, *A 19-mW 2.6mm2 L1/L2 Dual-Band CMOS GPS Receiver*, IEEE Journal of Solid-State Circuits, vol.40, no.7, pp.1414-1425, 2005.

[5] G. Gramegna, P. Mattos, M. Losi, S. Das, M. Fransciotta, N. G. Bellantone, M. Vaiana, V. Mandara, M. Paparo, *A 56-mW 23-mm2 Single- Chip 180-nm CMOS GPS Receiver with 27.2-mW 4.1-mm2 Radio*, IEEE Journal of Solid-State Circuits, vol.41, no.3, pp.540-551, 2006.

[6] T. Kadoyama, N. Suzuki, N. Sasho, H. Iizuka, I. Nagase, H. Usukubo, M. Katakura, *A Complete Single-Chip GPS Receiver with 1.6-V 24-mW Radio in 0.18um CMOS*, IEEE Journal of Solid-State Circuits, vol.39, no.4, pp.562-568, 2004.

[7] F. Chastellain, C. Botteron, P.-A. Farine, *A Low-Power RF Front-end for an L1/L2C GPS Receiver*, proc. of ION GNSS 2005, International conference on GPS and GNSS, Long Beach, CA, USA, pp. 628-634, 2006.

[8] K. P. Pun, J. E. da Franca, C. Azeredo Leme, R. Reis, *Quadrature Sampling Schemes with Improved Image Rejection*, IEEE Transactions on Circuits and Systems II, vol.50, no.9, pp.641-648, 2003.

[9] P. Leroux, J. Janssens, M. Steyaert, *A 0.8-dB NF ESD-Protected 9-mW CMOS LNA Operating at 1.23-GHz*, IEEE Journal of Solid-State Circuits, vol. 37, no.6, pp.760-765, 2002.